Real-time Ground Motion Prediction based on Data Assimilation using Front-site Waveform Information for the Application to Local Earthquake Early Warning

Mike Lindner (mike.lindner@student.kit.edu)
Geophysical Institute, Karlsruhe Institute of Technology, Kaiserstrasse 12, 76131 Karlsruhe, Germany

Masato MOTOSAKA (motosaka@irides.tohoku.ac.jp)
International Research Institute of Disaster Science, Tohoku University, Aramaki Aza-Aoba 468-1, Aoba-ku, Sendai 980-0845, Japan

In-time warning of strong shaking for affected citizens is one of the primary objectives of Earthquake Early Warning (EEW). To satisfy this requirement, EEW with a continuous front-site observation network and quick analyzing algorithm to ensure enough warning time are indispensable. For near site events, warning time is scarce and depends on a swift processing after the first recording. It is therefore crucial to prolong warning time and improve the overall quality of the warning. In this study, we use seismic energy transfer, which bases on the theory of ray scattering [11], to model a real-time numerical ground motion map by simulating point sources beneath the observation sites, using the observation as initial energy. Using nine independent prediction models based on geological data [4], it is now possible to provide models for spatial energy distribution in the near future, originating from each observation site. Furthermore, real-time evaluation and adjustment of the predicted field based on new observation has been realized by using data assimilation. The developed EEW system allows us to model an interpolated wave-field behind, and a predicted wave-field in front of the wave-front, thus providing ground motion information aside recording sites. The error of the predicted ground motion is in average less than 0.5 in JMA-Intensity and better for the assimilated wave-field.

Keyword: *Real Time, Earthquake Early Warning, Ground Motion Prediction, Frequency Prediction, Radiative Transfer Theory, Data Assimilation, Scattering*

Wave Scattering and Radiative Transfer Theory

The theory of radiative energy transfer (RTT) combines the attenuation and scattering characteristics of a wave field propagating through a heterogeneous subsoil media. While attenuation is expressed as an overall decline of amplitude per time, scattering describes the redirection of energy rays from an incident to an arbitrary propagation direction and governs the behavior behind the wave front, also known as wave coda [1]. To describe the resulting wave-field, we follow a model with spatial fluctuating velocity, caused by small scale inhomogeneous regions, around a constant background velocity V_0 as shown by Sato [11] [10]:

$$\underbrace{u(x,t)}_{\substack{\texttt{full}\\ \texttt{wave field}}} = \underbrace{u^0(x,t)}_{\substack{\texttt{mean}\\ \texttt{wave field}}} + \underbrace{u^1(x,t)}_{\substack{\texttt{scattered}\\ \texttt{wave field}}}$$

Aki and Chouet [1] defined a scattering coefficient g, describing the scattering behavior of a wave-field with above properties, which depends on the average distance an energy ray travels without experiencing redirection. Margerin [9] and Sato [11] explained the derivation of this coefficient in a well-arranged manner, for an energy amount dE passing through an unit area $d\sigma$ per unit time dt and brought it into a mathematical context, combining the correlation between wave front and coda phases with the overall attenuation per time:

$$E(\vec{x},t) = W_{\Delta t} G(\vec{x},t) + V_0 g_0 \iiint_{-\infty}^{\infty} G(\vec{x}-\vec{x}', t-t') E(\vec{x}', t') dt' d\vec{x}' \quad (1)$$

Equation 1 describes the full wave-field in two dimensions and depends on a spatial velocity and scattering model. The complex scattering process for the full field is modeled as a Greens-function which describes the redirection of energy rays from $\vec{x}'$ to $\vec{x}$. An approximated solution of Equation 1 for a multiple scattering regime is given by [11] with:

$$E(r,t) \approx \underbrace{\frac{W_{\Delta t}}{2\pi V_0 r} \delta\left(t - \frac{r}{V_0}\right) e^{-g(\vec{x})V_0 t}}_{\texttt{Wave Front}} + \underbrace{\frac{W_{\Delta t}}{4\pi D t} H\left(t - \frac{r}{V}\right) e^{-\frac{r^2}{4Dt}}}_{\texttt{Coda Wave}} \quad (2)$$

$$\text{with} \quad r = |\vec{x}| = \sqrt{x^2 + z^2} \text{ and } D = \frac{V_0}{2g(\vec{x})}$$

Hereby, the initial energy $W_{\Delta t} \propto 10^{I_{JMA,\Delta t}} \propto \ddot{u}_{3D,\Delta t,max}$, modeled as a finite impulse point source, is proportional to the JMA-Intensity that itself is a function of the peak ground acceleration (PGA) for a time period Δt. Delta function δ and step function H ensure causality while an exponential function governs attenuation. $V^0 = V^0_{P,S} = const.$ and $g(\vec{x},\omega) = g_{P,S}(\vec{x},\omega)$ are physical models describing the wave velocity and the scattering for compression waves (P-Wave) and shear waves (S-Wave). The scattering model $g(\vec{x},\omega)$ is calculated from an inhomogeneous velocity model $V_{P,S}(\vec{x},\omega) \neq V^0$ based on a geological model and frequency depended seismic quality factor $Q_{P,S}(\vec{x},\omega)$:

$$g_{P,S}(\vec{x},\omega) = \frac{\omega(f)}{Q_{P,S}(\vec{x},\omega) \cdot V_{P,S}(\vec{x}),\omega} \quad (3)$$

Data Assimilation

With ongoing time, the wave-front will reach a second station for which the energy was already predicted from a previous time step. To evaluate the prediction and correcting the energy distribution in correlation distance, data assimilation is used. This algorithm enables it to compare the predicted field $u^b_n \propto E(r,t)_n$ at time t_n with the actual observation $\nu_n \propto I_{JMA,n}$ and evaluates an error for it. We hereby follow the approach published by [7] using the optimal interpolation method. Equation 4 describes the energy field u^a_n after including observation information, with the predicted field u^b_n and an error term, that includes the deviation between the prediction and the observation $\Delta\nu_n$ and a weight matrix $\mathbf{W}$ at time step n.

$$\mathbf{u}^a_n = \underbrace{\mathbf{u}^b_n}_{Prediction} + \underbrace{\mathbf{W}\Delta\nu_n}_{Error} \quad (4)$$

Hereby, exponent b defines the predicted background field at time t_n without observation information which is a function of the previous assimilated field $\mathbf{u}^a_{n-1}$, that includes observational information, noted with a.

System algorithm

The region displayed in figure Fig*1* is the target area of this study, covering the Kyoshin-Network in Miyagi (MYG) operated by NIED [5].

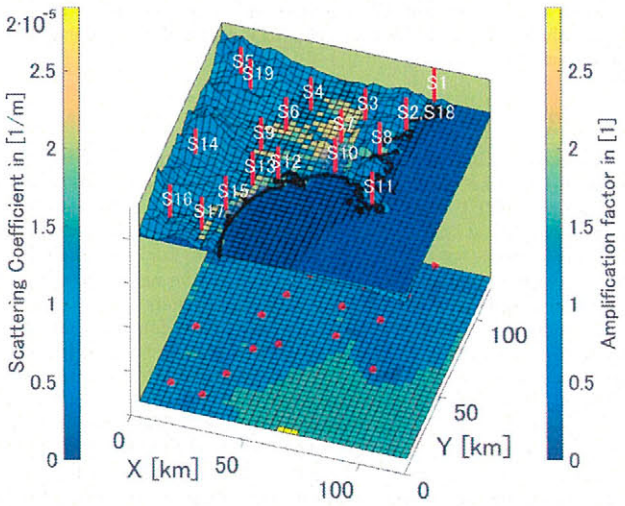

Fig1. Topographic research area including side amplification (upper layer) and P-Wave scattering (lower layer) information.

Colorized displayed in the upper layer is the local amplification map $\alpha(\vec{x},\omega)$ with a 3x3 km resolution adapted to the topographic surface structure for a frequency of $f = 1$ Hz at $V_{S30} = 400\frac{\text{m}}{\text{s}}$ [6] [4]. The lower layer shows the spatial variation of the scattering coefficient $g(\vec{x},\omega)$ in the bedrock, which was modeled following equation 3 for a frequency of $f = 1$ Hz [4] [2] [3]. As data, we are using strong motion wave forms provided by NIED [5] from subduction events with a moment magnitude between 5.7 to 6.5 offshore Miyagi Prefecture subdivided into north, south and east cluster to study directivity effects. Following the method of bedrock to surface transfer, RTT simulated the energy propagation in the bedrock, originating from a point source below an observation point, and is governed by a homogeneous velocity model with $V_P = 6\frac{\text{km}}{\text{s}}$ and $V_S = 3.4\frac{\text{km}}{\text{s}}$. The prediction model is hereby time independent and was calculated for each observation station for $t_{pred} = 30$ seconds and initial unit energy impulse of $W^0 = 1$. Prediction in a continuous system is done for each site i individuality dividing the observed surface intensity with the site amplification factor to obtain the seismic energy in the bedrock $W_{i,\Delta t,B} = \frac{W_{i,\Delta t,S}}{\alpha(\vec{x}_i,\omega)}$. The predicted surface intensity is then given with:

$$\mathbf{u}^b_{n,i} = \alpha(\vec{x},\omega) \cdot \left(\sum_i^I \Gamma_i \cdot W_{i,\Delta t,B} \cdot E_i(r, t_{pred.})\right) + (\mathbf{u}^a_{n-1,i} - \mathbf{u}^b_{n-1,i})/2\pi$$

whereby, Γ_i is introduced as time independent scaling factor to compensate for missing energy portion which is not considered due to approximation assumptions. The secondary term is introduced to correct the predicted field using past observation information [7]. The obtained predicted wave-fields are now merged by using a minimum distance approach, where the intensity at an arbitrarily point is a function of the nearest observation site. The resulting two dimensional field resembles a rag rug, whereby each region depends on the quality of the respected observation site. For a transient signal originating from a single source, this rag rug becomes a smoothed real-time map showing the spatial intensity distribution for up to $T_{pred} = 30$ seconds into the future aside the observation points. The predicted wave field is then used as background field $\mathbf{u}_n^b$ for the data assimilation to model an assimilated wave-field $\mathbf{u}_n^a$. This sequence is repeated for every $\Delta t = 0.3$ seconds. As result we obtained a real-time map, showing the interpolated intensity between the observation sites and the predicted wave-field apart the observation network.

Prediction results

Figure Fig*2* shows the prediction result for station **S3** and **S4** during an earthquake event with moment magnitude $M_w = 6.3$ on the 2011.07.24 in the southern area offshore Miyagi Prefecture at (37.730°N 141.390°E) and a depth of $Z = 40.0$ km. Figure Fig*3* shows the average error and standard derivation of the predicted and assimilated P- and S-Phase for 6 events, all having similar attributes. Stations **S9-S17** were used as front-site group with stations **S1-S8,S18** as target group. By predicting sites from the nearest observation point, stations **S1-S3,S7-S8** were predicted by Station **S10** while stations **S4-S6** depend on station **S9**. The displayed average error and corresponding standard derivation is calculated between the modeled and observed intensity. We hereby differ between the errors for P- and S-Phases. The P-Phase is defined in time from the P-Wave onset up to the maximum amplitude, which is assumed as S-Onset. The S-Phase then stretches in time from the defined S-Onset to the end of the modeled time frame of 60 seconds (compare figure Fig*2*). Figure Fig*3* therefore shows the mean average error in P and S-Wave of 6 events at the respected station.

Discussion

The proposed method can predicted the intensity in a circular area around a single observation point, with the radius depending on prediction time t_{pred} and V^0. RTT itself is used time independent and was calculated for each front-site station individually. The bedrock to surface interacting is modeled using a spatial scalar amplification factor $\alpha(\vec{x}, \omega)$ and scaling factor Γ_i, which is a function of distance from the respected observation station and should balance out the geometrical energy loss and reflected phases. With an average processing time of 0.002 seconds per 0.01 seconds sampling time per station, the proposed method can be used in real-time. These processing durations were achieved using Matlab R2016 on an Intel Core i7 Notebook using Windows 10. As for the prediction quality, we are able to produce a good accuracy of the S-Coda, which is mainly governed by scattering processes in the local surface. On the other hand, our prediction model has to deal with different simplification errors as well as neglecting any source information and path effect along the hypocenter and the first observation station. Furthermost, each front-site shows unique envelope shapes and especially varying P-Coda, which next to scattering also includes reflected wave phases from outside the target area. By neglecting source information, the quality of this method has also to deal with a too early S-Wave onset for large distance predictions, which originates form the travel time difference between P and S-Wave. While RTT is using impulse sources following Huygens Principle to produce P-Waves and S-Waves, we cannot model radiation characteristics from the source or reflection sources. Furthermore, we have yet to consider regional geological structures. Stations located in mountain areas (e.g. **S5, S14** and **S19**) or stations behind a mountain range (e.g. **S1, S2** etc. for events in the south) show significant different envelope shapes compared to stations in the plain (e.g. **S7, S9** or **S10**). Another geological characteristic we need to consider are the active fault zones extending from south west to north east throughout the target area. The fault zone can act as shallow reflector and could have an effect for predictions orthogonal to it. [8]. Lastly, we also have to consider random error originating from local noise or corrupt data files.

Further Work

The prediction depends so far mainly on the envelope shape and quality of single front-site stations. To increase the quality of the system, the algorithm needs to be expended to a wider frequency band for the geological models. Also, by including extern information about the source location, we want to tackle the problem of the too early S-Wave onset time.

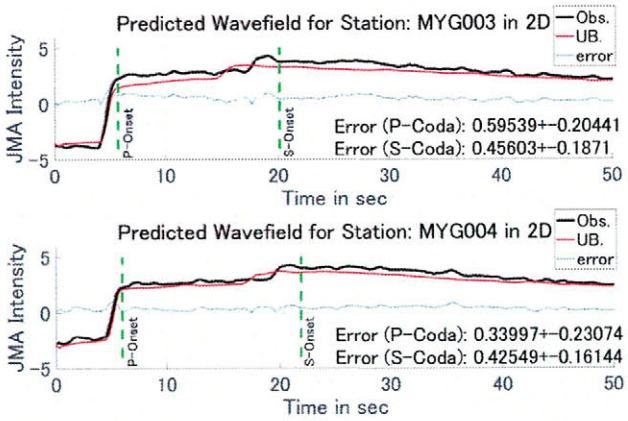

Fig2. **Top**: Prediction result at station **S3**. **Bottom**: Assimilation result for station **S4** during an earthquake event in the southern cluster.

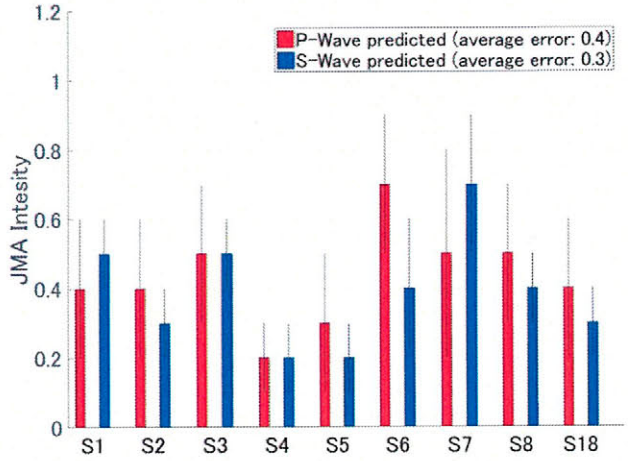

Fig3. Absolute average error and standard derivation between prediction and observation of P- and S-Wave for earthquake events with moment magnitude M5.8 to M6.5 located south of Miyagi Prefecture.

Acknowledgments

We thank NIED and J-SHIS for providing the wave form and geological data we used to conduct this study.

References

[1] Keiiti Aki and Bernard Chouet. Origin of coda waves: source, attenuation, and scattering effects. *Journal of geophysical research*, 80(23):3322–3342, 1975.

[2] H. Fujiwara et al. A study on subsurface structure model for deep sedimentary layers of japan for strong-motion evaluation. *Technical Note of the National Research Institute for Earth Science and Disaster Prevention*, 337, 2009.

[3] H. Fujiwara et al. Some improvements of seismic hazard assessment based on the 2011 tohoku earthquake. *Technical Note of the National Research Institute for Earth Science and Disaster Prevention*, 379, 2012.

[4] NIED (National Research Institute for Earth Science and Disaster Prevention). J-SHIS japan seismic hazard information station, 2014.

[5] NIED (National Research Institute for Earth Science and Disaster Prevention). Strong-motion Seismograph Networks k-net, kik-net, 2016.

[6] K. Fujimoto and S. Midorikawa. Empirical estimates of site amplification factor from strong-motion records at nearby station pairs. *Proceedings of the 1st European Conference on Earthquake Engineering and Seismology*, 251, 2006.

[7] Mitsuyuki Hoshiba and Shigeki Aoki. Numerical shake prediction for earthquake early warning: Data assimilation, real-time shake mapping, and simulation of wave propagation. *Bulletin of the Seismological Society of America*, 105(3):1324–1338, 2015.

[8] Kazutoshi Imanishi, Hisao Ito, Yasuto Kuwahara, Yutaka Mamada, Takanobu Yokokura, Naomi Kano, Kazuo Yamaguchi, and Akiko Tanaka. Deep structure of the nagamachi-rifu fault deduced from small aperture seismic array observations. *Earth, Planets and Space*, 54(11):1033–1038, 2002.

[9] Ludovic Margerin. Introduction to radiative transfer of seismic waves. *Seismic Earth: Array Analysis of Broadband Seismograms*, pages 229–252, 2005.

[10] Haruo Sato. Wave propagation in one dimensional inhomogeneous elastic media. *Journal of Physics of the Earth*, 27(6):455–466, 1979.

[11] Haruo Sato, Michael C Fehler, and Takuto Maeda. *Seismic wave propagation and scattering in the heterogeneous earth*, volume 496. Springer, 2012.